Full Paper

Propellants, Explosives, Pyrotechnics

DOI: 10.1002/prep.201900159

Rheological Considerations for Binder Development in Direct Ink Writing of Energetic Materials

Hannah Woods,[a] Andrew Boddorff,[a] Elena Ewaldz,[a] Zachary Adams,[a] Mitchell Ketcham,[a] Dong June Jang,[a] Elizabeth Sinner,[a] Naresh Thadhani,[a] and Blair Brettmann*[a, b]

Abstract: Additive manufacturing is a promising approach to prepare highly specifically defined materials with unique dimensions, gradients in material attributes and on-demand properties. For energetic materials applications, it is particularly exciting for its potential to create lattice and cellular structures and gradient solids to focus or dissipate energy. However, there are significant challenges to overcome, particularly in obtaining the very high particle content (>80 vol% particles), while still being manufacturable. This work focuses on the polymer binder used in an energetic materials system and aims to understand how its characteristics affect the viscosity and printability of the suspension. Two different types of polymer binders are examined: (a) high molecular weight polymer in a solvent and (b) polymerizable smaller molecules that were cured via UV light. We show that the suspension viscosity is primarily controlled by the particle volume fraction for the UV curable binder, while both the particle volume fraction and polymer molecular weight influence the response in the case of the polymer/solvent binder. Both binder types can be tuned to provide printable suspensions that result in lines of consistent width and 3D disc-shaped objects, indicating that both paths are good potential directions for future formulations for polymer bonded explosives prepared via additive manufacturing.

Keywords: Additive manufacturing · rheology · polymer · suspension · photopolymerization

1 Introduction

Additive manufacturing (AM) has been transformative for a number of industries, providing personalized medical implants [1–3], allowing for cost-effective prototyping [4], and improving production of specialized aerospace parts [5–7], among others. AM provides a unique opportunity to fabricate energetic materials in geometries that are traditionally difficult or impossible to manufacture via subtractive means, in particular engineered lattice and cellular structures for wave focusing or energy dissipation [8]. Though effort has been made to use AM to prepare energetic materials [9,10], the high solids loadings required for these materials provide significant challenges to processing, particularly for the most flexible method of AM, direct ink writing (DIW). DIW requires precise control of the precursor material under flow conditions, with the deposited material then solidifying to maintain its shape. This requires development of new binder systems for energetic materials formulations, particularly for polymer bonded explosives (PBX).

In DIW additive manufacturing, inks composed of particles, polymer binders, monomers, and organic solvents are extruded through a 3D printing nozzle. The materials solidify as the solvent evaporates or, if pre-polymer monomers are used, will solidify when exposed to heat or light (Figure 1). By depositing multiple filaments in a pre-defined pattern, a 3D solid structure is formed that contains particles suspended in a solid polymeric binder. High particle

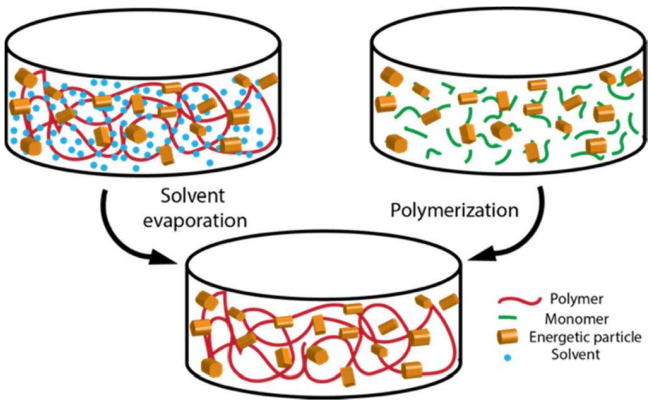

Figure 1. Illustration of the solvent evaporation and polymerization solidification processes for formation of high particle loading parts

[a] *H. Woods, A. Boddorff, E. Ewaldz, Z. Adams, M. Ketcham, D. J. Jang, E. Sinner, N. Thadhani, B. Brettmann*
School of Materials Science and Engineering, Georgia Institute of Technology, Atlanta, GA 30332, USA
[b] *B. Brettmann*
School of Chemical and Biomolecular Engineering, Georgia Institute of Technology, Atlanta, GA 30332, USA

Supporting information for this article is available on the WWW under https://doi.org/10.1002/prep.201900159

loadings are possible with DIW, including greater than 50 vol% [11], and a variety of complex structures can be formed [12]. The slurry used in DIW must be properly designed to have a homogeneous particle distribution, fast solidification kinetics, suitable rheology for flow and shape retention, and strong adhesion between the filaments [11]. In this work, we focus primarily on the rheology aspects of potential AM suspensions.

Current PBX formulations are highly loaded suspensions (HLS) of solid particles in a continuous phase, and the properties of these suspensions differ from more common situations such as dilute particle suspensions, where there is a high volume fraction of the continuous phase, and granular materials, where air is the continuous phase. Many studies on HLS examine smaller particle sizes than those relevant to PBX [13–15] and define "highly loaded" at a lower level, such as 40 vol% [16, 17]. There are limited studies that analyze the rheology of the HLS. In detailed rheological studies, the measured flow behaviors such as complex viscosity and storage and loss moduli as a function of shear stress, strain and frequency, provide insight into particle properties, matrix properties, particle-particle interactions, particle-matrix interactions, and the structure of the material (i.e. gel, solution, solid, etc.) [9, 14, 16, 18–20]. This provides a powerful toolset for characterizing HLS of energetic particles in matrix polymers for PBX.

In some cases, rheological properties have been measured for energetic HLS, including PBX and other energetic formulations. For example, mock energetic formulations containing pentaerythriol particles and polydimethyl siloxane (PDMS) binder at 80 vol% particle loadings [21], acrylonitrile butadiene (ABS) with acetone solvent and energetic materials at 50 vol% particle loadings [22], and three different Semtex formulations, typical PBX [23], have all been examined. The studies demonstrated that the formulations had a high viscosity and were shear thinning with a yield stress [21–23]. They were highly elastic fluids, with a storage modulus that was much larger than the loss modulus [22, 23]. These results indicate that the PBX behaves similarly to other HLS, but the studies do not thoroughly investigate the effects of binder properties, such as molecular weight and binder viscosity, on the rheology of the slurry.

In this work, we examine the rheological properties of two different types of binders for AM formulations for energetic materials. Two approaches to solidification of a HLS AM system are evaluated: solvent evaporation and polymerization (Figure 1). The polymerization-based method begins with a mixture of low molecular weight monomers and particles, followed by printing and initiation of a polymerization process that converts the monomers into cross-linked polymers post-extrusion, resulting in a solid part. The polymerization is typically initiated by heat or UV/visible light, allowing the monomers to remain stable during handling and printing, and only polymerizing when desired. In an evaporation-based system, a high molecular weight polymer is dissolved in a solvent and mixed with the particles. This slurry is printed and the solvent subsequently evaporates from the printed lines, resulting in a solid part. Here, we focus on a mixture of monomers that polymerize when exposed to UV light. These include bisphenol A-glycidyl methacrylate (Bis-GMA) and diethylene glycol dimethacrylate (TEGDMA), a binder system commonly used in highly loaded dental composites [24, 25]. We compare these to mixtures of polyvinyl pyrrolidone (PVP) and methanol, our representative system for the solvent evaporation approach, which we have previously used to electrospin high particle loading composites [26]. We tie the rheological properties to printability using a line width analysis and show that, when the composition of particles remains below the jamming concentration, either method is promising.

2 Experimental Section

2.1 Materials

PVP powders with molecular weights of 10,000 Da, 40,000 Da, 55,000 Da, and 1,300,00 Da were purchased from Millipore Sigma, methanol was purchased from VWR, the photocurable monomers Bis-GMA and TEGDMA were purchased from Millipore Sigma, and the photoinitiator 1-hydroxycyclohexyl phenyl ketone (commercially sold as Irgacure 184) was purchased from Millipore Sigma. Hollow glass spheres of reported 9–13 μm diameter were purchased from Millipore Sigma and used as model energetic particles.

2.2 Sample Preparation

Suspensions were prepared in 150 mL polypropylene cups or 20 mL glass scintillation vials, depending on the volume needed for the experiment. To prepare the solutions, we converted the target volume of particles (based on total volume of suspension desired) into mass percent using the reported particle density for the glass spheres used in this work (1.1 g/mL) and weighed the solids by mass to mix with a measured volume of solution. An example conversion is 10 mL particles * 1.1 g/mL = 11 g particles. The binder (either PVP/methanol or BisGMA/TEGDMA) was prepared in excess and allowed to mix under stirring overnight. The binder and the particles were then mixed in either 150 mL polypropylene (PP) cups or 20 mL glass vials in a Flacktek DAC400.2VAC-LR Programmable Speed Mixer for 3 min total at two speeds, first 30 s at 1000 rpm followed by 150 s at 1500 rpm. The short low speed mixing step was designed to wet the particles and incorporate them into the binder. The second step was optimized by running at 150 s at speeds ranging from 800 to 2300 rpm and measuring the temperature rise and viscosity. All conditions greater than 1100 rpm resulted in similar variations in viscosity, indicating similar homogeneity, while speeds greater than

1500 rpm displayed further temperature increases (by a few degrees Celsius with each 100 s of rpm increase), so 1500 rpm was chosen as the condition with acceptable mixing while minimizing the temperature increase.

These times and speeds were optimized to ensure quality mixing with minimal increase in the temperature. For the solvent-based mixtures, two layers of parafilm were used to cover the cups/vials during mixing to minimize solvent evaporation during the mixing process.

Samples were taken for rheological testing after at least 20 min of cooling and with no more than 8 hours passing after the final mixing step. For printing, the suspension was transferred to a 30 mL BD plastic syringe and degassed in the Flacktek mixer for 60 seconds at 1500 rpm, prior to printing within 6 hours.

2.3 Structure-Property Characterization

2.3.1 Particle Size Measurements

The particle size of the hollow glass particles was verified using laser diffraction with a Malvern Analytical Particle Sizer 3000 with a wet dispersion module (Hydro EV accessory). Measurements were taken under constant mixing (via the built-in propeller in the instrument) and sonication was done for ~30 seconds prior to starting the measurements.

2.3.2 Scanning Electron Microscopy

Samples were observed using a Zeiss Ultra60 (Carl ZeissNTS, LLC North America) field emission scanning electron microscope (FE-SEM) at a 3–5 kV operating voltage. Samples were mounted with carbon tape on aluminum stubs and sputter coated with a Hummer 6 gold/palladium sputter coater.

2.3.3 Rheology

Complex viscosity and storage and loss moduli of the highly loaded suspensions were measured using a TA Instruments DHR-3 rheometer with 20 mm cross-hatched parallel plates and Peltier plate. The initial geometry gap was set to 1 mm and the solvent trap was in place, with axial force adjustment at 0.05 N compression. Oscillation frequency tests were run at 0.01 % strain on all suspensions to characterize the viscoelastic behavior. This strain value was specifically selected using basic strain sweep data to ensure experiments would remain within the linear viscoelastic regime of the suspensions.

The binders alone (PVP/methanol and Bis-GMA/TEGDMA) were characterized using the TA Instruments DHR-3 rheometer with a strain sweep test in the linear viscoelastic region to determine the zero shear viscosity.

2.3.4 DIW Line Tests and 3D Objects

All prints were performed using a Hyrel Hydra 640 3D printer and SDSXT-30 printer head (which uses a stepping motor with a gear reduction system) with 14G Nordson Smooth-Flow Tapered Luer nozzles. For the line tests, we used a motor speed of 30 pulse/μL and a head speed of 5 mm/s to deposit a snaking single layer line pattern (Figure 2–A) onto

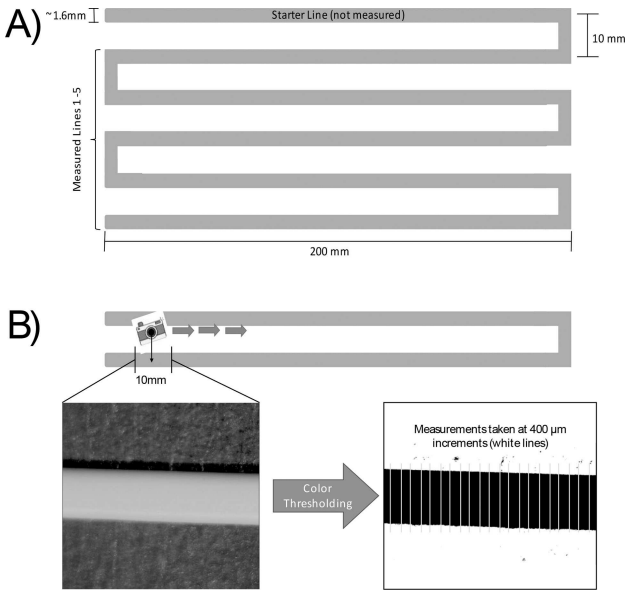

Figure 2. A) Pattern of deposited lines used to measure the consistency of the line width. The layer height is 1 mm. B) Depiction of the imaging process showing an example of a raw (left) and thresholded image (right) used for pixel counting.

a transparent plastic sheet in order to analyze the variation of the width of the deposited material. Before the print starts, the extruder performs a short, fast extrusion called a prime action that pushes material into the syringe tip and begins extrusion. The printer head then moves 200 mm extruding material in a straight line with a layer height of 1 mm. At the end of the first line, the printer head moves perpendicularly for 10 mm then prints the same 200 mm line parallel to the initial print. This repeats until all lines are deposited. The whole print is done without interruption. Upon finishing the print, the head is moved off to the side and an unprimed action is performed (opposite of a prime) to stop the extrusion of material. For the UV binder system, the lines are then cured with a 365 nm UV light pen that retraces the printing path. The GCODE for this DIW extrusion process is included in the supplementary information.

In order to measure the width, images are taken of each line in 10 mm segments. The resultant images are color thresholded with ImageJ in order to segment the image (Figure 2-B). Approximately every 400 μm, the pixels across

the line are counted as shown by yellow lines in Figure 2–B. A calibration slide is used for each set of images to convert the pixels to microns.

2.3.5 Flow Tests

We have developed a simple test to examine how the suspension flow changes throughout the printing process and to allow for easy comparison between different systems and formulations without running full rheological studies. The mass extruded in a 42 second time window, which corresponds to one line of the printing line tests, is collected in weigh boats and measured immediately. Prior to the first 42 second run, the syringe is primed for 0.53 seconds. We perform multiple 42 second runs for each formulation, corresponding to the lines in the line tests, and examined how the mass extruded in 42 seconds changes from the start to end of the experiment. The GCODE for the flow tests is in the supplementary information.

3 Results and Discussion

3.1 Material Characterization

Particle size and the particle size distribution play an important role in the rheological properties of a suspension, particularly at high loadings. Small particles will have a higher viscosity than large particles at the same composition due to increased particle-particle interaction through the higher surface area [16, 21]. For this study, we are using hollow glass spheres with a reported diameter of 9–13 μm. Figure 3 shows an SEM image (A) and the particle size distribution as measured using laser scattering (B). The particle size distribution is monomodal with a D50 of 11.7 μm and a D90 of 23.0 μm.

In addition to the properties of the particles, the rheology of the binder system plays a role in the rheology of the suspensions used for printing, though the interplay between binder rheology and suspension rheology is less clear. Table 1 lists the viscosity of the binders in the linear region of the viscosity versus angular frequency experiments for four different PVP molecular weights (at 30 vol%/ 39.4 wt% PVP in methanol). Table 2 lists the viscosity for the pure monomers and 4 different ratios of Bis-GMA:TEGDMA, the compositions used in this study. Both binder systems cover a wide range of viscosities, with PVP solutions ranging from 0.0196 to 366.6 Pa s and the UV curable monomers ranging from 0.0072 to 637.4 Pa s. This provides us with a broad basis over which to develop binders for AM.

The viscosity of the PVP solution increases as the molecular weight increases (Figure 4–A), with a particularly high viscosity obtained at 1300k molecular weight, which is typical for polymer solutions [27]. For the UV curable monomer system, the viscosity increases with increasing amounts of the more viscous component, Bis-GMA, with an almost linear trend of log(viscosity) versus weight percent of Bis-GMA (Figure 4–B). This is to be expected, as there is no entanglement in these monomers, and the relationship between composition and viscosity will be close to a simple average of the two components.

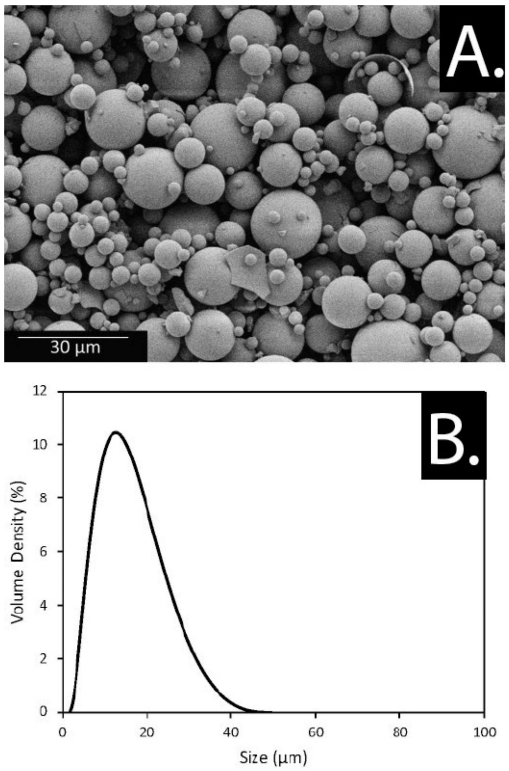

Figure 3. A) SEM micrograph and B) laser diffraction measurements showing the particle size distribution of hollow glass particles

Table 1. Viscosity of the solvent evaporation binders.

Polymer	Solvent	Vol% polymer in solvent	Viscosity (Pa.s)
10,000 Da PVP	Methanol	30	0.0196 +/− 0.0009
40,000 Da PVP	Methanol	30	0.1082 +/− 0.0035
55,000 Da PVP	Methanol	30	0.1200 +/− 0.0060
1,300,000 Da PVP	Methanol	30	366.6 +/− 24.5

3.2 Effect of Particle Loading on Rheology and Line Printing

To study the effect of particle loading on the suspension rheology, we prepared HLS containing 61–68 vol% particles in a moderate molecular weight PVP (55k). This range of particle loadings was selected because it is most relevant for our application, and we used the 30 vol% PVP in methanol binder to correspond with the studies on rheology of

Table 2. Viscosity of the polymerization binders. Vol% and wt% Bis-GMA and vol% photointiator are listed for each sample. The balance is TEGDMA.

Sample name	Vol % Bis-GMA	Wt % Bis-GMA	Wt % photo-initiator	Viscosity (Pa.s)
TEGDMA	0	0	1	637.4 +/− 16.5
1:2 Bis-GMA: TEGDMA	31.68	33	1	5.592 +/− 0.158
1:1 Bis-GMA: TEGDMA	48.01	50	1	0.9600 +/− 0.0306
2:1 Bis-GMA: TEGDMA	64.66	67	1	0.1605 +/− 0.0069
4:1 Bis-GMA: TEGDMA	78.24	80	1	0.0479 +/− 0.0012
Bis-GMA	100	100	1	0.0072 +/− 0.0008

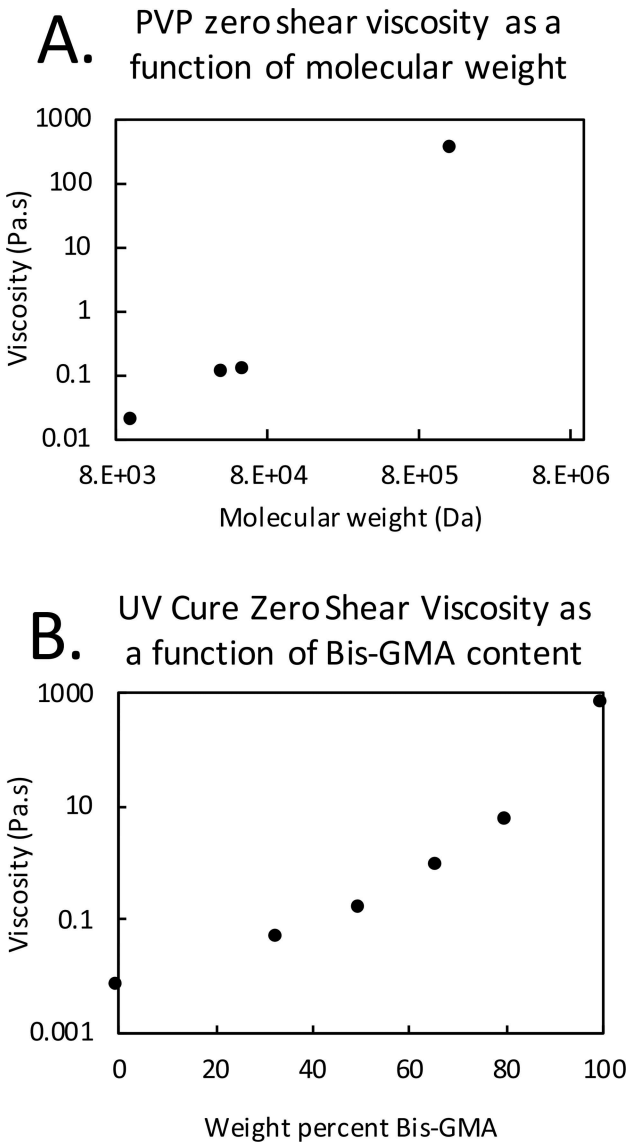

Figure 4. Zero shear viscosity of binder materials: A) viscosity versus molecular weight for the PVP binders and B) viscosity versus weight percent of Bis-GMA for the UV cure binders

the binders. Figure 5–A shows the viscosity measured at 1 rad/s for each vol% particle composition. The jamming transition is clearly visible through the increase in viscosity at approximately 67 vol% particles. This corresponds well to the theoretical jamming transition at 0.64 volume fraction for random close-packed spheres [28], and likely differs due to our particle size distribution not being uniformly monomodal [29]. DIW line printing illustrates that below the jamming transition, the suspension was printable (results will be discussed in further sections), but above the jamming transition, the particle suspensions were not printable with the printer set-up and motor. This indicates that a formulation should be selected with a volume fraction below approximately 66% for monomodal 10 μm spheres when using the PVP/methanol 55k binder suspension. For further studies, we will use 61.4 vol% particles, which are well within the lower viscosity range below the jamming transition.

A similar study was performed with the mixture of Bis-GMA and TEGDMA UV curable monomers (Figure 5–B). As with the PVP/methanol binder, the viscosity plateaus at high volume percent particles corresponding to the jamming transition for 10 μm hard spheres. What is notable with the UV-curable monomers in contrast to the PVP is the clear trend of increasing viscosity starting at lower (61–66) volume percents with less scatter in the results. This may be due to evaporation occurring in the PVP samples that is hard to control. With so little solvent in these suspensions, even a small amount of evaporation can lead to strong increases in the viscosity and lead to the scatter seen in the PVP binder samples (Figure 5–A). Future use of the binders containing solvents may need to carefully design a mixing process that fully prevents solvent evaporation to maintain controllable rheology for printing.

3.3 Effect of Polymer Molecular Weight for Solvent Evaporation System

For a given polymer concentration in a solvent, an increase in the molecular weight will increase the viscosity of the

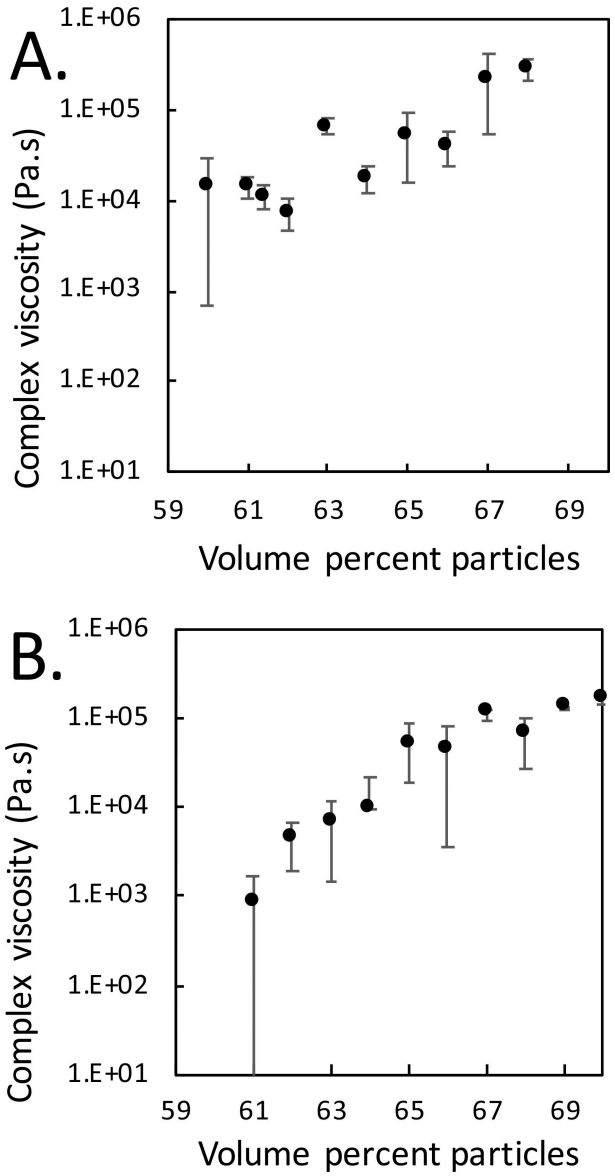

Figure 5. Viscosity at 1 rad/s as a function of volume percent particles for A) the 30 vol% PVP in methanol binder and B) the 2:1 Bis-GMA:TEGDMA binder.

solution. At very high concentrations, entanglements between polymer chains increase this effect even more. In the presence of high particle loadings, the increase in viscosity due to the increase in the polymer molecular weight is still present, as can be seen in Figure 6, which shows the complex viscosity of 61.4 vol% hollow glass spheres in a 30 vol% PVP in methanol binder. For the 10k PVP molecular weight, the viscosity displays a value of 563 Pa.s at 1 rad/s, while viscosity at 1 rad/s increases to 4.3×10^5 Pa.s for 1300k PVP, three orders of magnitude higher.

The viscosity of the 1300k PVP is extremely high, so we examined the flow of these different solutions in the syringe/nozzle using the flow tests described previously. Figure 7 shows the extrusion rate plotted against the line number (corresponding to the line tests) for the 10k, 55k and 1300k PVP in Figure 7. It is clear from these results that the 1300k PVP is not printable. The extrusion rate increases over the first 4 lines, but then decays off as the print continues, always staying below about 0.05 g/min. The 10k and 55k PVP reach the steady state extrusion rate of 0.2 g/min by the second line and maintain that flow rate up to 23

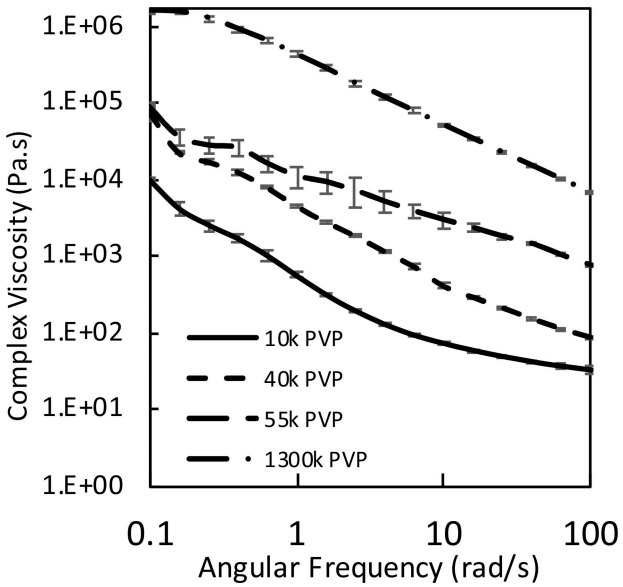

Figure 6. The viscosity of 61.4 vol% particles in 30 vol% PVP in methanol binder for five different polymer molecular weights, 10k (solid), 40k (short dashed), 55k (long dashed) and 1300k (dash dot)

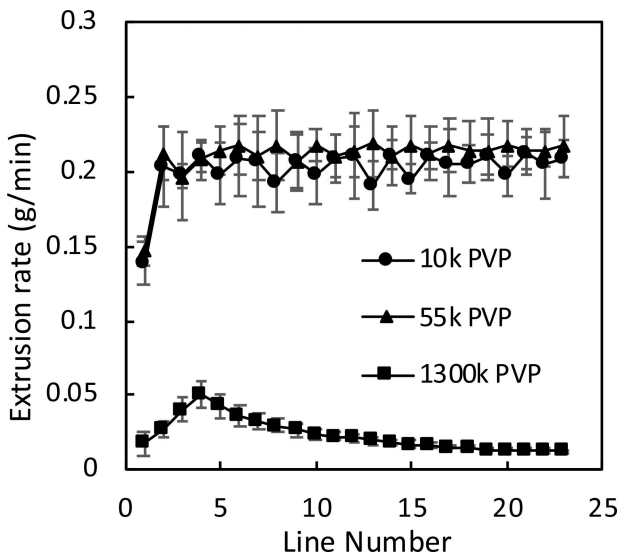

Figure 7. Extrusion rate as a function of the line number printed for 61.4 vol% particle suspension with three different PVP solutions (30 wt% PVP in methanol, 10k (circle), 55k (triangle) and 1300k (square)

lines, indicating that they are good candidates for printing with respect to flow rate consistency.

3.4 Effect of Ratio of Bis-GMA to TEGDMA

Since Bis-GMA has a viscosity that is two orders of magnitude higher than TEGDMA, we saw a significant increase in the viscosity of the binders when the amount of Bis-GMA was increased (Figure 4–B). To determine the effect of this on the suspension rheology, we examined four different ratios, 1:2, 1:1, 2:1 and 4:1 Bis-GMA:TEGDMA with 61.4 vol% particles. As can be seen in Figure 8, there is a slight increase in the viscosity as the amount of Bis-GMA in the mixture increases, but it is barely significant given the size of the error bars. Specifically, the 4:1 Bis-GMA:TEGDMA is significantly different than the 1:1 and 1:2, but it is within error of the 2:1 Bis-GMA:TEGDMA. This indicates that, for these mixtures of monomers with particles, the particle behavior is the primary driver for how the suspension flows, in contrast to the behavior seen with the high molecular weight polymers in solvents.

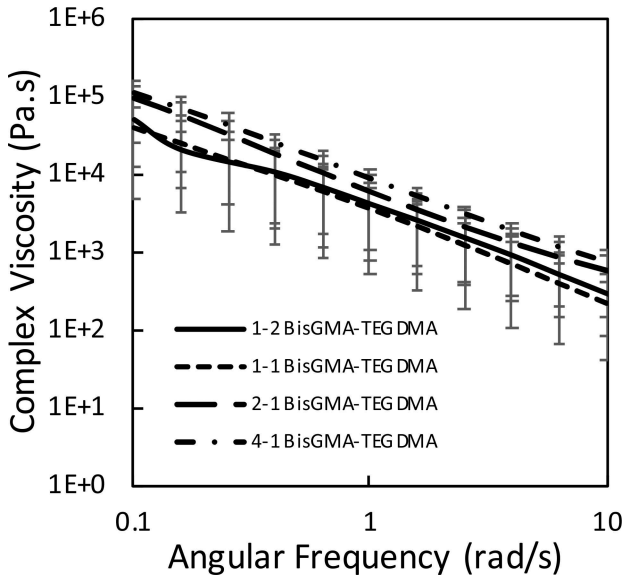

Figure 8. The viscosity of 61.4 vol% particles in a mixture of Bis-GMA and TEGDMA at four different ratios, 1:2 (solid), 1:1 (short dash), 2:1 (long dash) and 4:1 (dash dot) Bis-GMA:TEGDMA

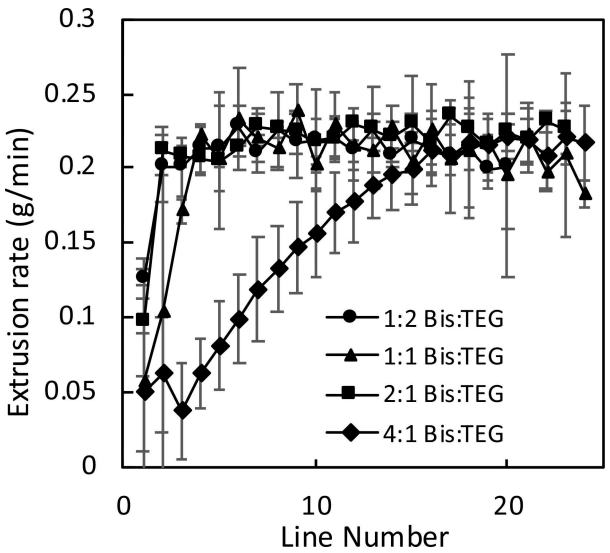

Figure 9. Extrusion rate as a function of the line number printed for 61.4 vol% particle suspension in a mixture of Bis-GMA and TEGDMA at four different ratios, 1:2 (circle), 1:1 (triangle), 2:1 (square) and 4:1 (diamond) Bis-GMA:TEGDMA

Flow tests were performed on the four different ratios of Bis-GMA to TEGDMA and these are plotted in Figure 9. For all three lower Bis-GMA ratios, steady state was reached relatively quickly, by about lines 3–5, while for the highest ratio of Bis-GMA:TEGDMA, steady state was not reached until line 17. The cause of the different behavior for the 4:1 sample is unknown, though it is not caused by aging of the sample as all 3 repeats, which were done consecutively with the same syringe, showed similar behavior. As the 2:1 Bis-GMA:TEGDMA showed acceptable start-up behavior and consistent flow and it is known from the literature to be a good ratio for curing [24, 25, 30], we move forward with this mixture for further testing.

3.5 Comparison of the Solvent Evaporation and Polymerization Binders in Print Tests

A major objective of this work is to understand the difference in the rheology and flow of the selected solvent evaporation and polymerization binders (PVP/methanol versus Bis-GMA/TEGDMA). To do this, we examined the printability, represented by the flow tests and line tests to compare the two systems, particularly focusing on the 61.4 vol% particle cases. We used the 55k PVP (30 vol% in methanol) binder since it had moderate viscosities over the range tested and showed good consistency in the flow tests. It was also noted that it was cohesive enough to allow effective syringe loading and seemed to print well. For the UV cure system, we used the 2:1 Bis-GMA:TEGDMA, which is known in the literature to be a good ratio for curing [24, 25, 30]. The viscosities of the two are compared in Figure 10–A. Interestingly, the two formulations show similar viscosities, despite being selected for properties other than viscosity. They diverge at higher angular frequencies, with the Bis-GMA/TEGDMA mixture showing a lower viscosity.

To examine their printability, we performed line tests for these two formulations. The average line width over lines 2–7 (we removed line 1 to focus on the steady state regime) was 0.79 +/− 0.08 mm for 55k PVP (30 vol% in methanol) and 0.99 +/− 0.14 mm for 2:1 Bis-GMA:TEGDMA when

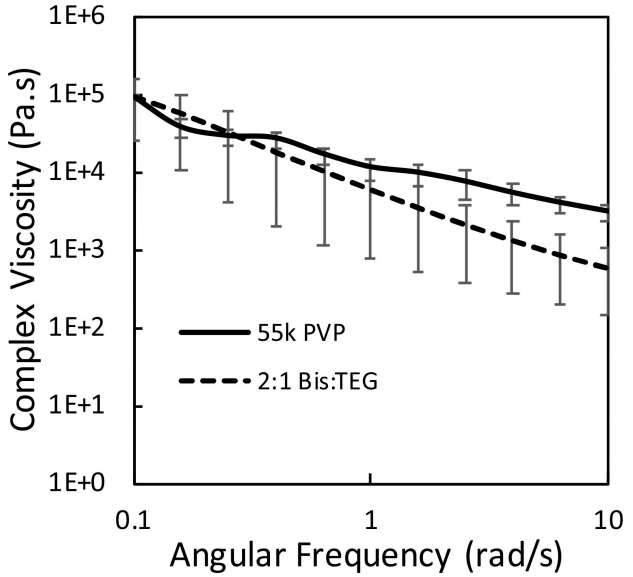

Figure 10. The viscosity as a function of angular frequency for 61.4 vol% particles in 55k PVP (30 vol% in methanol) binder (solid) and 2:1 Bis-GMA:TEGDMA (dash)

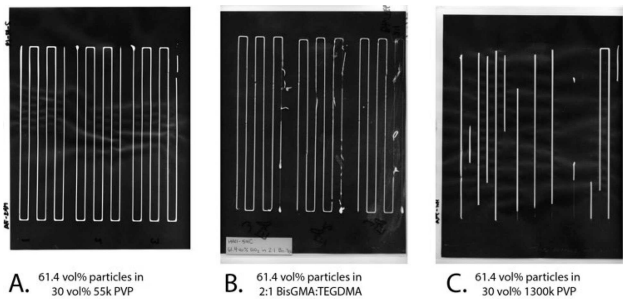

Figure 11. Line prints of A) 61.4 vol% particles in 55k PVP (30 vol% in methanol), B) 61.4 vol% particles in 2:1 Bis-GMA:TEGDMA and C) 61.4 vol% particles in 1300k PVP (30 vol% in methanol)

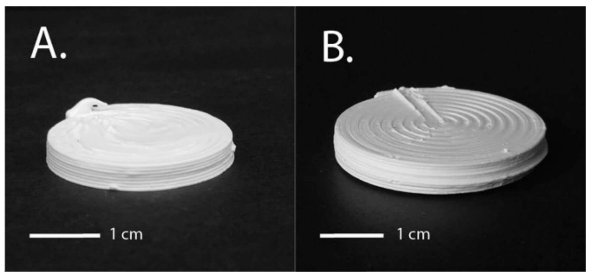

Figure 12. DIW printed discs made from A) 61.4 vol% particles in 55k PVP binder (30 vol% in methanol) and B) 61.4 vol% particles in 2:1 Bis-GMA:TEGDMA binder

printed with our 1.6 mm nozzle. This shows that the printing is relatively consistent from one line to another (only varying by 10% and 14% for PVP and Bis-GMA/TEGDMA, respectively) throughout the print. However, the line width measurements ignore areas of significant defects and only take into account the smooth printing areas. In the case of the two binders tested here, the visual quality of the prints were significantly different. As shown in Figure 11–A&B, the first 2–3 lines of the Bis-GMA/TEGDMA sample have significantly more defects. The initial hypothesis is that there is less cohesion in the jet due to a lack of entanglements, leading to easier breakage for the Bis-GMA/TEGDMA. For comparison, Figure 11–C also shows the print for the very high molecular weight PVP (1300k). It is clear that the print quality was poor, as less than half of the printing was successful. This corresponds with flow test data that show a low extrusion rate for the 1300k PVP formulation, limiting the amount of material coming out of the syringe.

DIW was also used to print 3D shapes in the form of discs (~30 mm diameter and 4–6 mm thick) using 61.4 particle suspensions for the 55k PVP (30 vol% in methanol) and 2:1 Bis-GMA:TEGDMA are shown in Figure 12 A and B, respectively. Both cylinders are similar with no obvious voids, but significant surface heterogeneity on the sides and top from the printing path. These were printed with non-optimized printing parameters, but show the promise of these materials for additive manufacturing of solid 3-dimensional objects.

We also examined the surface of the printed objects at the microscale using SEM (Figure 13). Images were analyzed using ImageJ software and converted to binary images using the Threshold function. The color threshold was set so

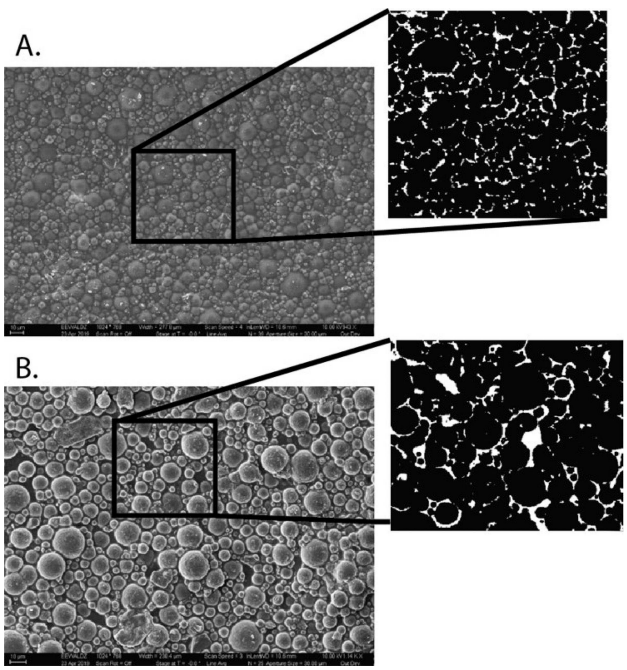

Figure 13. A) SEM micrograph of the surface of a print from 61.4 vol% particles in 55k PVP binder (30 vol% in methanol) and B) SEM micrograph of the surface of a print from 61.4 vol% particles in 2:1 Bis-GMA:TEGDMA binder

that the particles were shown as black and the binder shown as white. This was repeated for the 2–1 Bis-GMA/TEGDMA system. The percentage of black area compared to white area in the image was calculated to determine the percentage area of particles. It was found that the areas were similar between the two systems, 89.6% for 2:1 Bis-GMA:TEGDMA and 91.0% for 55k PVP. The main differences seen are the spacing between particles, with 55k PVP system having less space between particles, but appearing to have more small particles on the surface. In the 2:1 Bis-GMA:TEGDMA system, we see larger particles along with larger spacing between particles. We believe this difference in spacing and particle size distribution is due to a difference in curing mechanisms/time scales. With solvent evaporation, the system solidifies very quickly so the polymer and particles get locked into place immediately after printing. Whereas with a UV curing system, the sample is left uncured for a certain amount of time before being treated with UV light. This allows time for relaxation of the system and movement of particles, with smaller particles being more mobile in the matrix and settling to the substrate surface.

4 Conclusion

This work examined the rheology and printability of highly loaded silica particle suspensions in two different types of polymer binders: a high molecular weight polymer in a solvent and polymerizable smaller molecules that were cured via UV light. In both cases, the suspensions could be tuned to a printable viscosity, in the range of 1 x 10^4-1 x 10^5 Pa.s at 1 rad/s angular frequency and printed as lines of consistent width, as well as 3D objects in the form of discs. For the high molecular weight polymer binder, 30 vol% PVP in methanol, the molecular weight had a strong effect on both binder viscosity and suspension viscosity. This is contrary to the UV curable binder system, Bis-GMA/TEGDMA, where the ratio of the monomers only affected the binder viscosity and the particle loading primarily set the suspension viscosity. In both cases, the viscosity increased with volume fraction of particles up to approximately 67 vol%, where the jamming transition occurrs and the viscosity plateaued at a high value. These results show a flexible formulation system for preparing highly loaded suspensions of energetic particles, creating a path to the design of new, high performance energetic materials, including polymer bonded explosives.

Acknowledgements

This work was supported by DTRA grant number HDTRA1-18-1-0004. DJJ was supported by an Undergraduate Research Scholarship provided by Novelis. This work was performed in part at the Georgia Tech Institute for Electronics and Nanotechnology, a member of the National Nanotechnology Coordinated Infrastructure, which is supported by the National Science Foundation, United States (Grant ECCS-1542174). The authors would also like to acknowledge Dr. Kimberly Kurtis and Xenia Wirth at Georgia Tech for their generous use of the particle size analyzer, Manali Banerjee for SEM images of particles and Didier Montaigne, AFRL-Eglin, for many valuable consultations.

References

[1] C. L. Ventola, Medical Applications for 3D Printing: Current and Projected Uses, *P. T.* **2014**, *39*, 704.
[2] R. J. Morrison, S. J. Hollister, M. F. Niedner, M. G. Mahani, A. H. Park, D. K. Mehta, R. G. Ohye, G. E. Green, Mitigation of tracheobronchomalacia with 3D-printed personalized medical devices in pediatric patients, *Sci. Transl. Med.* **2015**, *7*.
[3] S. J. Hollister, C. L. Flanagan, R. J. Morrison, J. J. Patel, M. B. Wheeler, S. P. Edwards, G. E. Green, Integrating Image-Based Design and 3D Biomaterial Printing To Create Patient Specific Devices within a Design Control Framework for Clinical Translation, *ACS Biomater. Sci. Eng.* **2016**, *2*, 1827.
[4] S. Junk, M. Tränkle, Design for additive manufacturing technologies: New applications of 3d-printing for rapid prototyping and rapid tooling, *ICED 11–18th International Conference on Engineering Design* **2011**, pp. 12–18.
[5] J. M. Waller, B. H. Parker, K. L. Hodges, E. R. Burke, J. L. Walker, Nondestructive Evaluation of Additive Manufacturing, *State-of-the-Discipline Report*, **2014**.
[6] R. Liu, Z. Wang, T. Sparks, F. Liou, J. Newkirk, *13 – Aerospace Applications of Laser Additive Manufacturing*, Elsevier Ltd, **2016**.
[7] A. Uriondo, M. Esperon-Miguez, S. Perinpanayagam, The present and future of additive manufacturing in the aerospace sector: A review of important aspects, *Proc. Inst. Mech. Eng. Part G* **2015**, *229*, 2132.
[8] Z. Ozdemir, E. Hernandez-Nava, A. Tyas, J. A. Warren, S. D. Fay, R. Goodall, I. Todd, H. Askes, Energy absorption in lattice structures in dynamics: Experiments, *Int. J. Impact Eng.* **2016**, *89*, 49.
[9] M. J. Mezger, K. J. Tindle, M. L. Pantoya, L. Groven, D. M. Kalyon, *Energetic Materials: Advanced Processing Technologies for Next-Generation Materials*, CRC Press, **2018**.
[10] F. Ruz-Nuglo, L. Groven, J. A. Puszynski, Additive Manufacturing for Energetic Components and Materials, in *50th AIAA/ASME/SAE/ASEE Joint Propulsion Conference*, American Institute of Aeronautics and Astronautics, Reston, Virginia, **2014**, pp. 1–7.
[11] N. Travitzky, A. Bonet, B. Dermeik, T. Fey, I. Filbert-Demut, L. Schlier, T. Schlordt, P. Greil, Additive Manufacturing of Ceramic-Based Materials, *Adv. Eng. Mater.* **2014**, *16*, 729.
[12] A. E. Jakus, S. L. Taylor, N. R. Geisendorfer, D. C. Dunand, R. N. Shah, Metallic Architectures from 3D-Printed Powder-Based Liquid Inks, *Adv. Funct. Mater.* **2015**, *1*.
[13] M. Acosta, V. L. Wiesner, C. J. Martinez, R. W. Trice, J. P. Youngblood, Effect of Polyvinylpyrrolidone Additions on the Rheology of Aqueous, Highly Loaded Alumina Suspensions, *J. Am. Ceram. Soc.* **2013**, *96*, 1372.
[14] T. Chu, J. W. Halloran, High-temperature flow behavior of ceramic suspensions, *J. Am. Ceram. Soc.* **2000**, *83*, 2189.
[15] T. Kaully, A. Siegmann, D. Shacham, Rheology of highly filled natural $CaCO_3$ composites. I. Effects of solid loading and particle size distribution on capillary rheometry, *Polym. Compos.* **2007**, *28*, 512.

[16] M. M. Rueda, M.-C. Auscher, R. Fulchiron, T. Périé, G. Martin, P. Sonntag, P. Cassagnau, Rheology and applications of highly filled polymers: A review of current understanding, *Prog. Polym. Sci.* **2017**, *66*, 22.
[17] F. Soltani, U. Yilmazer, Slip velocity and slip layer thickness in flow of concentrated suspensions, *J. Appl. Polym. Sci.* **1998**, *70*, 515.
[18] J. S. Chong, E. B. Christiansen, A. D. Baer, Rheology of concentrated suspensions, *J. Appl. Polym. Sci.* **1971**, *15*, 2007.
[19] A. Kristoffersson, R. Lapasin, C. Galassi, Study of interactions between polyelectrolyte dispersants, alumina and latex binders by rheological characterization, *J. Eur. Ceram. Soc.* **1998**, *18*, 2133.
[20] D. M. Kalyon, An Overview of the Rheological Behavior and Characterization of Energetic Formulations: Ramifications on Safety and Product Quality, *J. Energ. Mater.* **2006**, *24*, 213.
[21] M. Sweeney, L. L. Campbell, J. Hanson, M. L. Pantoya, G. F. Christopher, Characterizing the feasibility of processing wet granular materials to improve rheology for 3D printing, *J. Mater. Sci.* **2017**, *52*, 13040.
[22] B. Clark, Z. Zhang, G. Christopher, M. L. Pantoya, 3D processing and characterization of acrylonitrile butadiene styrene (ABS) energetic thin films, *J. Mater. Sci.* **2016**, *52*, 993.
[23] M. Hoffman, H. Turner, A. Racoveanu, Fourier Transform Rheology of Paste Explosives: I. Semtex Formulations, *JANNAF Meeting* **2013**, 1.
[24] N. B. Cramer, J. W. Stansbury, C. N. Bowman, Recent Advances and Developments in Composite Dental Restorative Materials, *Crit. Rev. Oral Biol. Med.* **2011**, *90*, 402.
[25] P. K. Shah, J. W. Stansbury, Role of filler and functional group conversion in the evolution of properties in polymeric dental restoratives, *Dent. Mater.* **2014**, *30*, 586.
[26] E. Ewaldz, R. Patel, M. Banerjee, B. K. Brettmann, Material selection in electrospinning microparticles, *Polymer* **2018**, *153*, 529.
[27] W. R. Krigbaum, P. J. Flory, Molecular weight dependence of the intrinsic viscosity of polymer solutions. II, *J. Polym. Sci.* **1953**, *11*, 37.
[28] S. Torquato, T. M. Truskett, P. G. Debenedetti, Is random close packing of spheres well defined?, *Phys. Rev. Lett.* **2000**, *84*, 2064.
[29] H. J. H. Brouwers, Particle-size distribution and packing fraction of geometric random packings, *Phys. Rev. E* **2006**, *74*, 863.
[30] C. Charton, V. Falk, P. Marchal, F. Pla, P. Colon, Influence of Tg, visocsity and chemical structure of monomers on shrinkage stress in light-cured dimethyacrylate-based dental resins, *Dent. Mater.* **2007**, *23*, 1447.

Manuscript received: May 10, 2019
Revised manuscript received: August 8, 2019
Version of record online: October 8, 2019

